2002

Theoretical Predictions of Electromechanical Deformation of Cells Subjected to High Voltages for Membrane Electroporation

R. P. Joshi
Old Dominion University

Q. Hu
Old Dominion University

K. H. Schoenbach
Old Dominion University

H. P. Hjalmarson

Original Publication Citation

Joshi, R. P., Hu, Q., Schoenbach, K. H., & Hjalmarson, H. P. (2002). Theoretical predictions of electromechanical deformation of cells subjected to high voltages for membrane electroporation. *Physical Review E, 65*(2), 021913. doi:10.1103/PhysRevE.65.021913

Theoretical predictions of electromechanical deformation of cells subjected to high voltages for membrane electroporation

R. P. Joshi, Q. Hu, and K. H. Schoenbach
Department of Electrical and Computer Engineering, Old Dominion University, Norfolk, Virginia 23529-0246

H. P. Hjalmarson
Computational Biology and Materials Technology Department, Sandia National Laboratory, Albuquerque, New Mexico 87185-1111
(Received 24 September 2001; published 25 January 2002)

An electromechanical analysis based on thin-shell theory is presented to analyze cell shape changes in response to external electric fields. This approach can be extended to include osmotic-pressure changes. Our calculations demonstrate that at large fields, the spherical cell geometry can be significantly modified, and even ellipsoidal forms would be inappropriate to account for the deformation. Values of the surface forces obtained from our calculations are in very good agreement with the 1–10 mN/m range for membrane rupture reported in the literature. The results, in keeping with reports in the literature, demonstrate that the final shape depends on membrane thickness. This has direct implications for tissues in which significant molecular restructuring can occur. It is also shown that, at least for the smaller electric fields, both the cellular surface area and volume change roughly in a quadratic manner with the electric field. Finally, it is shown that the bending moments are generally quite small and can be neglected for a simpler analysis.

DOI: 10.1103/PhysRevE.65.021913 PACS number(s): 87.15.Aa, 87.50.Rr, 87.50.−a, 87.17.Aa

I. INTRODUCTION

Electroporation is a well-known physical process in biological cells [1–3]. It involves rapid structural rearrangement of the membrane, in response to an externally applied electric field. The field is not an ac excitation, and typically quasistatic. The most prominent observable effect is a rapid increase in the electrical conductivity by several orders of magnitude [4]. This is attributed to the formation of aqueous pathways, or pores, in the lipid bilayer of the membrane. The opening of such channels (or more appropriately, transient aqueous pores) enables the transport of ions and water-soluble species both into and out of individual cells. Electroporation can, therefore, be used to initiate large molecular fluxes for purposes of introducing genetic material into cells, manipulation of cells and tissues, and other applications in biotechnology [5–9].

Electroporation has also been linked to the nonthermal killing of micro-organisms subjected to strong electric fields [10]. For this reason, it offers great potential for decontamination and the elimination of harmful micro-organisms and biohazards. Traditionally, most electroporation studies have focused on relatively low external voltages applied over extended time periods ranging from several tens of microseconds to milliseconds [11]. Recently, work has focused on the use of much shorter pulses (durations well below the microsecond range), but with electric fields as high as 100 kV/cm [12–15]. There appear to be several fundamental advantages in using short electric pulses for cellular manipulation. First, negligible thermal heating of the biological matter can be expected to occur due to the short-time duration. Much lower energies are required for pulsed inputs, and yet large values of the electric fields and peak powers can be obtained [16]. Also, pulsed fields afford a way by which the time scales can easily be manipulated.

Given the utility, it becomes important to understand and accurately analyze the field-assisted electroporation process. A necessary first step is the self-consistent electric-field calculation at the cell membrane and its spatial dependence. This is important since the field magnitude controls the pore formation rate, the evolution of the pore distribution function in ''r space'' as governed by the Smoluchowski equation [17,18], and ionic flow. However, electric fields are distorted by the polarizability of the biological medium and influenced by factors such as cellular size and geometric shape. For example, cigar-shaped cells have a greater ''field screening effect'' than spherically symmetric cells [19]. As is well known, biological cells can undergo pronounced changes in geometry and size [20–22] when subjected to external electric fields. The shape directly affects the electrical and mechanical properties of cells (such as capacitance and membrane tension, respectively), and dictates the location at which electromagnetic boundary conditions have to be applied. Shape-related changes in the mechanical properties are known to play an important part in physiology and cell biology [23]. For example, the membrane elasticity determines the flow properties of red blood cells, while shape-related variations in membrane tension can affect motility, control endo- and exocytosis and can even lead to extensive metabolic changes [24]. It therefore, becomes important to correctly account for the geometric changes and cellular deformations. The push towards high electric fields makes this germane issue even more important.

In general, there are two different mechanisms for volume and shape changes in cells upon the application of an external electric field. In one, excessive buildup of the potential (due to redistribution of the internal cellular charge) causes membrane perforations. Ionic flows then lead to imbalances in the osmotic pressure [25] and volume change results. Since this occurs after membrane perforation, a relative time delay is involved for this process. The studies by Hotani [26] using dark-field light microscopy on liposomes are typical examples. The other mechanism is associated with changes produced by mechanical forces arising from the Maxwell

stress tensor [27]. This process occurs prior to membrane rupture or cellular material flows, and hence, must be taken into account as an initial condition for electroporative analysis. Experimental observations of absorbance dichroism and changes in optical scattering associated with vesicle deformation of lipids are appropriate recent examples [28].

The subject of cellular deformation is not new, and has been studied by several researchers in the past. For example, Evans applied continuum mechanical deformation theory in the elastic limit for studying the problem of micropipette aspiration [29]. Their group assumed that the bending modulus was negligible in comparison to the shear modulus [30], an approximation that was included in subsequent analyses as well [31,32]. However, other treatments of membrane phenomena, such as the formation of tethers [33,34], spicules [35], and undulatory excitations [36] took the opposite view and emphasized bending stiffness of the membrane. Energy methods based on the principle of virtual work have also been used to predict cellular deformations [22,37–39]. However, approximations have been made to simplify the analysis. For example, it has often been assumed that the cellular shapes take on simple forms, such as ellipsoids of revolution [22,28,40,41]. However, as is well known, a wide variety of shapes other than ellipsoids are possible [38]. Others have invoked conditions of either constant surface area or fixed cell volume (incompressibility), or both, in their calculations [22,23,29] which strictly are invalid for deformable bodies. Finally, the electric energy in these calculations has often been based on a simple thin-walled, spherical-cell geometry, and typically ignore self-consistent analyses that could account for the role of geometric changes on the electric field, and hence, the Maxwell tensor.

In this contribution, the issue of calculating cell deformations self consistently due to the electromechanical forces is revisited. Use of an energy-based virtual work formalism is difficult for the treatment of dissipative forces and/or for nonequilibrium situations. So here an approach based on thin-shell theory [42,43] has been used, without applying constraints on surface area or cell volume as has typically been done in the past. Both the shear and bending moduli are carefully included in these ''small deformation'' calculations. The Love-Kirchhoff hypothesis (e.g., [44]), which states that ''normals'' to the center surface of a shell element remain perpendicular when the surface undergoes curvature, is invoked. The present calculations demonstrate that both the cellular surface area and volume change in response to an externally applied electric field, and roughly have a quadratic dependence. The angular distributions of the stress across the cell membrane have been obtained. Based on this analysis, the critical electric-field threshold for membrane rupture and the elastic limit can be ascertained directly. Bending moments are shown to be small. Finally, deviations from an ellipsoidal shape are demonstrated, underscoring the incorrectness of an assumed simple ellipsoidal shape.

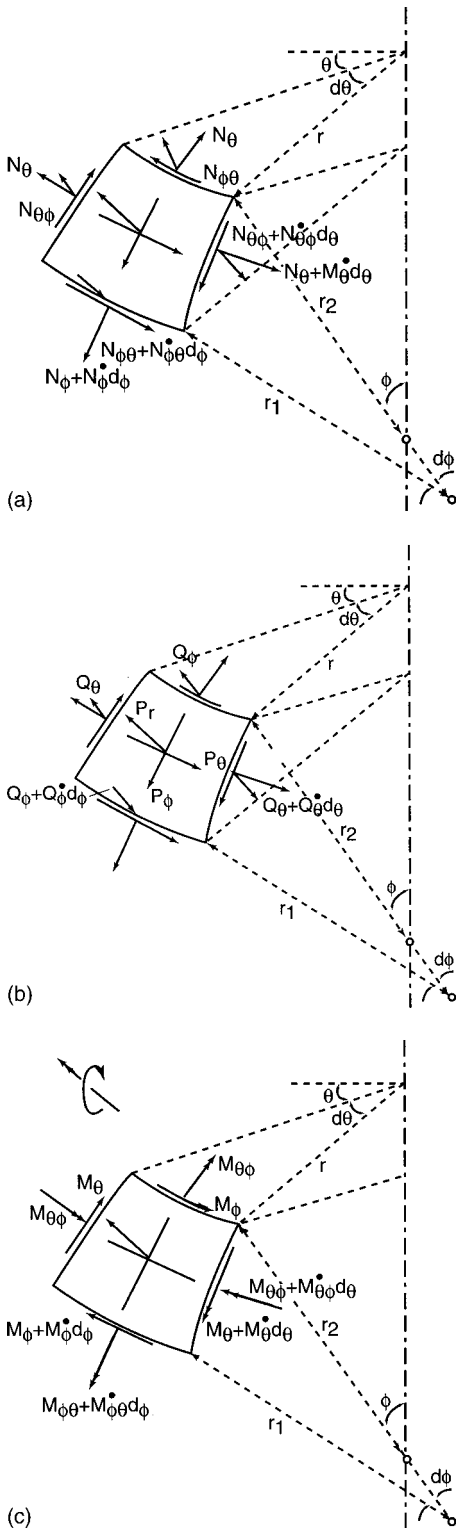

FIG. 1. Schematic of a typical thin shell element and the associated forces and moments. (a) The forces $N_{\theta\phi}$, N_θ, N_ϕ; (b) Q_θ, Q_ϕ, p_r, p_θ, p_ϕ; and (c) the moments $M_{\theta\phi}$, M_ϕ, and M_θ.

II. MODEL DETAILS

A. Stress and deformation

Our basic stress model is based on the classical small deformation theory of thin, elastic shells [42]. Since the thickness of cell membranes is on the order of 5 nm, compared to their radii of ~ 1 μm, the shell theory is quite appropriate. The forces and moments acting on a typical shell element are given in Fig. 1. Two meridians and two parallel circles, each indefinitely close together, have been shown.

Following the notation of Flugge [42], ϕ is the angle between a normal to the shell and its axis of revolution, while θ is the meridional angle. Also, N_ϕ denotes the meridional force per length, N_θ the hoop force per length, and $N_{\phi\theta}$ the shear. Furthermore in Fig. 1, p_r, p_ϕ, and p_θ are the externally imposed stresses (which could include internal osmotic pressure), while r is the distance from the axis of rotation, r_1 the radius of curvature, and r_2 the distance of intersection of the radius of curvature and the axis of revolution. In the present context, p_r, p_ϕ, and p_θ will be nonzero due to the presence of the Maxwell stress tensor associated with the external field. It is assumed that the osmotic pressure contributions to p_r, p_ϕ, and p_θ are negligible compared to the Maxwell stress produced by the high electric fields. From the geometry, $r=r_2\sin(\phi)$, while the elemental distance ''ds'' along the meridian is given by: $\mathrm{ds}=r_1\,d\phi$. Finally, M_ϕ, M_θ, and $M_{\phi\theta}$ are the bending moments (dimensions of force), while Q_θ and Q_ϕ are the transverse forces per length that arise from bending theory. At equilibrium, the balance of all forces and moments yields the following six equations:

$$d\{rN_\phi\}/d\phi + r_1 d\{N_{\theta\phi}\}/d\theta - r_1 N_\theta \cos(\phi) - rQ_\phi = -rr_1 p_\phi, \tag{1a}$$

$$d\{rN_{\phi\theta}\}/d\phi + r_1 d\{N_\theta\}/d\theta + r_1 N_{\theta\phi}\cos(\phi) - r_1 Q_\theta \sin(\phi) = -rr_1 p_\theta, \tag{1b}$$

$$r_1 N_\theta \sin(\phi) + rN_\phi + r_1 dQ_\theta/d\theta + d\{rQ_\phi\}/d\phi = rr_1 p_r, \tag{1c}$$

$$d\{rM_\phi\}/d\phi + r_1 d\{M_{\theta\phi}\}/d\theta - r_1 M_\theta \cos(\phi) = rr_1 Q_\phi, \tag{1d}$$

$$d\{rM_{\phi\theta}\}/d\phi + r_1 d\{M_\theta\}/d\theta + r_1 M_{\theta\phi}\cos(\phi) = rr_1 Q_\theta, \tag{1e}$$

$$M_{\phi\theta}/r_1 - M_{\theta\phi}/r_2 = N_{\phi\theta} - N_{\theta\phi}. \tag{1f}$$

The current problem of interest, involves a determination of the equilibrium stresses and moments on cells subjected to external electric, and the final deformed geometry under steady-state conditions. Here, there is an inherent axial symmetry along the direction of the applied electric field, and the behavior along the two axes transverse to the applied electric-field direction, will be identical. Such axial symmetry will hold for spherical cells at all times, and ellipsoidal (and other) shapes in the steady state after the cells have had the time to reorient themselves in response to the external field [45]. A sketch of the applied field and the geometric cell model is shown in Fig. 2. There is an inner region, the cell membrane shell, and the outer region. Though a spherical geometry is shown for simplicity, the shapes could be different, in general, with a symmetry perpendicular to the field direction. For such axisymmetric cases, the derivatives with respect to the angle θ drop out, while the shearing forces $N_{\phi\theta}$ and $N_{\theta\phi}$, the twisting moments $M_{\theta\phi}$ and $M_{\phi\theta}$, and the transverse shear Q_θ all vanish. Also, the load component p_θ is zero. Consequently, the following simpler set of equations result:

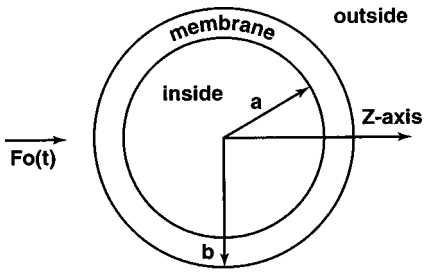

FIG. 2. Simple cellular geometry, showing axial symmetry, for field calculations.

$$d\{rN_\phi\}/d\phi - r_1 N_\theta \cos(\phi) - rQ_\phi = -rr_1 p_\phi, \tag{2a}$$

$$r_1 N_\theta \sin(\phi) + rN_\phi + d\{rQ_\phi\}/d\phi = rr_1 p_r, \tag{2b}$$

$$d\{rM_\phi\}/d\phi - r_1 M_\theta \cos(\phi) = rr_1 Q_\phi. \tag{2c}$$

The above three equations contain five unknowns, and need to be supplemented by the stress-strain relationships. In the elastic regime, the stresses can be related to the displacements v (transverse) and w (normal) in the following manner [42]:

$$N_\phi = (12K/t^2)[\{dv/d\phi + w\}/r_1 + \nu\{v\cos(\phi) + w\sin(\phi)\}/r], \tag{3a}$$

$$N_\theta = (12K/t^2)[\{v\cos(\phi) + w\sin(\phi)\}/r + \nu\{dv/d\phi + w\}/r_1], \tag{3b}$$

$$M_\phi = (K/r_1)[d(\{dw/d\phi\}/r_1)/d\phi + \nu\{d[\cos(\phi)\{dw/d\phi\}/r]/d\phi\}], \tag{3c}$$

$$M_\theta = (K/r_1)[\cos(\phi)\{dw/d\phi\}/r] + \nu[d(\{dw/d\phi\}/r_1)/d\phi], \tag{3d}$$

where K is the flexural rigidity (i.e., bending stiffness), ν the Poisson's ratio, t the shell thickness assumed to be a constant, and w and v the displacements due to deformation along the radial and angular directions. Equations (3a)–(3d) involve the displacements w and v that constitute two additional unknowns of the problem. Thus, the combined set of equations [2(a)–2(c)] and [3(a)–3(d)] yield a system of seven equations for the seven unknowns that can be solved.

In general, a numerical computation is required for obtaining a solution to the above problem. However, analytical expressions can be obtained under certain simplifying conditions. For example, consider the case: $M_\phi \sim M_\theta \sim Q_\phi \sim 0$ which corresponds to neglecting the bending forces and moments as has been proposed in the past [30–32]. Assuming that the external stresses arise solely from the Maxwell stress tensor associated with the applied external field (i.e., ignoring internal cell pressure and polarization effects), the stresses p_ϕ and p_r for the axisymmetric cases take the following form:

$$p_r = 0.5\varepsilon_0[k_{r1} - k_{r2}]E^2\cos(2\phi) \equiv F\cos(2\phi), \tag{4a}$$

and

$$p_\phi = -0.5\varepsilon_0[k_{r1}-k_{r2}]E^2 \sin(2\phi) \equiv -F\sin(2\phi), \tag{4b}$$

where E is the externally applied electric field, k_{r1} and k_{r2} the dielectric constants of the membrane and external medium, ε_0 the permittivity of free space ($=8.85\times10^{-12}$ F/m), and $F\equiv 0.5\varepsilon_0\,[k_{r1}-k_{r2}]\,E^2$. Using Eq. (4) in the equation set (2)–(3) yields the following simplifying solutions:

$$N_\phi(\phi) = [F/\{r_2\sin^2(\phi)\}] \times\left\{ {}_0\int^{\phi} r_1 r_2[\cos(2\phi^*)\cos(\phi^*)\sin(\phi^*) + \sin(2\phi^*)\sin^2(\phi^*)]d\phi^*\right\}, \tag{5a}$$

$$N_\theta(\phi) = r_2 F\cos(2\phi) - [r_2/r_1]N_\phi, \tag{5b}$$

$$v(\phi) = {}_0\int^{\phi}[q(\phi^*)/\sin(\phi^*)]d\phi^*, \tag{5c}$$

where

$$q(\phi)\equiv\{t^2/[12K(1-\nu^2)]\}\{r_1[N_\phi(\phi)-\nu N_\theta(\phi)] - r_2[N_\theta(\phi)-\nu N_\phi(\phi)]\}, \tag{5d}$$

and

$$w(\phi) = r_2\{t^2/[12K(1-\nu^2)]\}[N_\theta(\phi)-\nu N_\phi(\phi)] - v(\phi)\cot(\phi). \tag{5e}$$

For an initial spherical shape, $r_1=r_2=$ the radius "a," and the above simplifies to

$$N_\phi(\phi) = 0.5aF;\quad N_\theta(\phi) = aF[0.5-2\sin^2(\phi)], \tag{6a}$$

$$v(\phi) = -\{Fa^2t^2[12K(1-v)]\}\sin(2\phi), \tag{6b}$$

and

$$w(\phi) = \{Fa^2t^2[12K(1-v^2)]\}[0.5-2\sin^2(\phi) - v/2+2(1+v)\cos^2(\phi)]. \tag{6c}$$

For an ellipsoidal shape with "a" being the semimajor axis along the field direction, and "b" the semiminor axes in the two transverse directions (as has often been used in the literature), r_1 and r_2 take on the following expressions:

$$r_1 = (a^2/b)[\{1+\tan^2(\phi)\}/\{a^2/b^2+\tan^2(\phi)\}]^{1.5}, \tag{7a}$$

and

$$r_2 = \{b/\cos(\phi)\}[a^2/b^2+\tan^2(\phi)]^{-0.5}. \tag{7b}$$

Using Eqs. (7a) and (7b) into the equation set (5a)–(5e) then yields the complete solution for the ellipsoidal geometry.

B. Electric field analysis

In the above formulas, polarization effects were not considered and so the field was taken to equal the external electric field E given in terms of the factor F of Eq. (4a). However, given the presence of the cell and its membrane which are both polarizable materials, one needs to solve the Laplace equation to self-consistently determine the electric-field value and its spatial characteristics for assessing the Maxwell stress tensor. We first show this for a simple spherical-cell geometry as given in the schematic of Fig. 2. Both the spherical and ellipsoidal geometries lend themselves to analytical solutions, and hence, are chosen here as typical examples. Other simple geometries can also be analyzed numerically. The inner region has radius "a" and permittivity $\varepsilon_{\rm in}$. The applied electric-field F_0 was taken to be along the z axis. The cellular membrane of Fig. 2 has a thickness "$b-a$"="t" and permittivity $\varepsilon_{\rm mem}$, while the outer suspension region a permittivity of $\varepsilon_{\rm out}$. Due to azimuthal symmetry, the potentials in the three regions, which must satisfy the Laplace equation, can be expressed in terms of Legendre polynomials as

$$U_{\rm in}(r) = A_0P_0 + A_1rP_1 + A_2r^2P_2 + \cdots = \Sigma_{j=0,\infty}A_jr^jP_j, \tag{8a}$$

$$U_{\rm mem}(r) = \Sigma_{j=0,\infty}[B_jr^jP_j + C_jP_j/r^{j+1}], \tag{8b}$$

and

$$U_{\rm out}(r) = -F_0rP_1 + \Sigma_{j=0,\infty}D_jP_j/r^{j+1}, \tag{8c}$$

where $U_{\rm in}(r)$, $U_{\rm mem}(r)$, and $U_{\rm out}(r)$ are the potentials at the inside, membrane, and outer regions, P_j is the jth order Legendre polynomial, and F_0 the externally applied electric field. Also, A_j, B_j, C_j, and D_j are the coefficients of the Legendre series expansions that can be determined by applying matching boundary conditions at the interfaces of the three regions. Invoking continuity in the potential and displacement vector, then leads to the following boundary conditions:

$$U_{\rm in}(r=a) = U_{\rm mem}(r=a), \tag{9a}$$

$$U_{\rm mem}(r=b) = U_{\rm out}(r=b), \tag{9b}$$

$$\varepsilon_{\rm in}[\partial U_{\rm in}(r)/\partial r]|_{r=a} = \varepsilon_{\rm mem}[\partial U_{\rm mem}(r)/\partial r]|_{r=a}, \tag{9c}$$

and

$$\varepsilon_{\rm mem}[\partial U_{\rm mem}(r)/\partial r]|_{r=b} = \varepsilon_{\rm out}[\partial U_{\rm out}(r)/\partial r]|_{r=b}. \tag{9d}$$

The neglect of conductivity terms in Eq. (9) above merits clarification. The Maxwell tensor cell deformation calculations discussed here are important to simulate conditions prior to membrane rupture and material outflows. Deformation and the buildup of internal stresses have to be taken into account to mimic the initial phase for electroporative analysis. Under these conditions, the conductivity of the cellular system is small. Hence, the membrance conductivity is al-

most negligible and can be omitted. Straightforward, but tedious manipulation of Eq. (9) yields the following expressions for the potentials:

$$U_{\rm in}(r)=C_1(r/a^3)\cos(\phi)[1+\{2\varepsilon_{\rm mem}+\varepsilon_i\}/\{\varepsilon_{\rm mem}-\varepsilon_{\rm in}\}], \tag{10a}$$

$$U_{\rm mem}(r)=C_1\cos(\phi)[1/r^2+(r/a^3)\times\{2\varepsilon_{\rm mem}+\varepsilon_i\}/\{\varepsilon_{\rm mem}-\varepsilon_{\rm in}\}], \tag{10b}$$

$$U_{\rm out}(r)=-F_0\cos(\phi)[r-b^3/r^2]+\{C_1/r^2\}\cos(\phi)\times[1+(b/a)^3\{2\varepsilon_{\rm mem}+\varepsilon_{\rm in}\}/\{\varepsilon_{\rm mem}-\varepsilon_{\rm in}\}], \tag{10c}$$

where

$$C_1=-3F_0\varepsilon_{\rm out}/[\{T\varepsilon_{\rm mem}/a^3\}-2\varepsilon_{\rm mem}/b^3]+\{2\varepsilon_{\rm out}/b^3\}\times[1+(b/a)^3T], \tag{10d}$$

and

$$T=\{2\varepsilon_{\rm mem}+\varepsilon_{\rm in}\}/\{\varepsilon_{\rm mem}-\varepsilon_{\rm in}\}. \tag{10e}$$

Consequently, the electric fields $F_r(r)$ and $F_\phi(r)$ just outside the membrane (i.e., at $r=b_+$) are given as

$$F_r(r=b)=[3F_0+2(C_1/b^3)\{1+(b/a)^3\}]\cos(\phi)\equiv\mathbf{F}_r\cos(\phi), \tag{10f}$$

$$F_\phi(r=b)=[C_1/b^3]\sin(\phi)[1+(b/a)^3T]\equiv\mathbf{F}_\phi\sin(\phi). \tag{10g}$$

For $\varepsilon_{\rm in}=\varepsilon_{\rm mem}=\varepsilon_{\rm out}$, the above equations reduce to: $U(r)=-F_0r\cos\phi$), $F_r(r)=F_0\cos(\phi)$, and $F_\phi(r)=-F_0\sin(\phi)$.

While both $F_r(r=b)$ and $F_\phi(r=b)$ retain the $\cos(\phi)$ and $\sin(\phi)$ angular dependence, respectively, their magnitudes (i.e., $\mathbf{F}_r$ and $\mathbf{F}_\phi$) are altered by the presence of dielectric materials. The resultant field $|F|$ is no longer the z axis (i.e., not at an angle ϕ with respect to the normal). Instead, $|F|=[\mathbf{F}_r^2\cos^2(\phi)+\mathbf{F}_\phi^2\sin^2(\phi)]^{0.5}$, while the angle α between the resultant field $|F|$ and the normal becomes: $\alpha=\tan^{-1}[-\tan(\phi)\mathbf{F}_\phi/\mathbf{F}_r]$. Consequently, the expressions in Eqs. (4) get modified to the form: $p_r=0.5\varepsilon_0[k_{r1}-k_{r2}]|F|^2\cos(2\alpha)\equiv F^*\cos(2\alpha)$, and $p_\phi=-0.5\varepsilon_0[k_{r1}-k_{r2}]|F|^2\sin(2\alpha)\equiv -F^*\sin(2\alpha)$. Under these conditions, Eqs. (5a)–(5b) correspondingly change to

$$N_\phi(\phi)=[F^*/\{r_2\sin^2(\phi)\}]\times\left\{\int_0^\phi r_1r_2[\cos(2\alpha^*)\cos(\phi^*)\sin(\phi^*)+\sin(2\alpha)\sin^2(\phi^*)]d\phi^*\right\}, \tag{11a}$$

$$N_\theta(\phi)=r_2F^*\cos(2\alpha)-[r_2/r_1]N_\phi,\quad \text{where}\quad \alpha^*=\tan^{-1}[-\tan(\phi^*)\mathbf{F}_\phi/\mathbf{F}_r]. \tag{11b}$$

For an ellipsoidal geometry (a shape known to approximate many cells under deformation), the Laplace equation is most easily solved by resorting to ellipsoidal coordinates. We assume a prolate spheroid without loss in generality, with semimajor axis "a," semiminor axes "b," and center at the origin. The foci are taken to be along the z direction (parallel to the applied E field) at $(0,0,\pm L)$ with $L=[a^2-b^2]^{0.5}$. The eccentricity "e" then is given by: $e=L/a$. The coordinates ς, η, ϕ for this system are defined in the usual manner [46] with respect to the Cartesian coordinates as

$$z=L\varsigma\eta,\quad y=L[\{\varsigma^2-1\}\{1-\eta^2\}]^{0.5}\sin(\theta),\quad x=L[\{\varsigma^2-1\}\{1-\eta^2\}]^{0.5}\cos(\theta), \tag{12a}$$

i.e.,

$$\varsigma=[\{x^2+y^2+(z+L)^2\}^{0.5}+\{x^2+y^2+(z-L)^2\}^{0.5}]/(2L)\,\theta=\tan^{-1}(y/x),$$

and

$$\eta=[\{x^2+y^2+(z+L)^2\}^{0.5}-\{x^2+y^2+(z-L)^2\}^{0.5}]/(2L). \tag{12b}$$

The ellipsoidal surface then corresponds to a constant ς value given by: $\varsigma\equiv\varsigma_o=a/L$. Due to angular symmetry, the potentials in the three regions can be written as

$$U_{\rm out}(\varsigma,\eta)=-F_0L\varsigma\eta+A\varsigma Q(\varsigma),\quad U_{\rm mem}(\varsigma,\eta)=-BF_0L\varsigma\eta+C\varsigma Q(\varsigma), \tag{13a}$$

$$U_{\rm in}(\varsigma,\eta)=DF_0L\varsigma\eta,\quad \text{with}\quad Q(\varsigma)=0.5\zeta{\rm Ln}|(1+\varsigma)/(1-\varsigma)|-1, \tag{13b}$$

where A, B, and C are constants to be determined from the boundary conditions. Using the continuity of the potential and displacement vector across the inner and outer membrane (assumed to have constant thickness, "t"), results in the following solution:

$$U_{\rm out}(\varsigma,\eta)=-F_0L\varsigma\eta+A\varsigma Q(\varsigma), \tag{14a}$$

$$U_{\rm mem}(\varsigma,\eta)=A\eta[\varsigma Q(\varsigma_o)/\varsigma_o+(S_1/S_2)\times\{Q(\varsigma_o)/\varsigma_o-\{dQ(\varsigma_o)/d\varsigma\}(\varepsilon_{\rm out}/\varepsilon_{\rm mem})\}]+F_0L\eta[(S_1/S_2)(\varepsilon_{\rm out}/\varepsilon_{\rm mem}-1)-\varsigma], \tag{14b}$$

with

$$S_1=Q(\varsigma)-\varsigma Q(\varsigma_o)/\varsigma_o,\quad S_2=Q(\varsigma_o)/\varsigma_o-dQ(\varsigma_o)/d\varsigma, \tag{14c}$$

$$U_{\rm in}(\varsigma,\eta)=A\eta\varsigma[Q(\varsigma_o)/\varsigma_o+(S_3/S_2)\{Q(\varsigma_o)/\varsigma_o-\{dQ(\varsigma_o)/d\varsigma\}(\varepsilon_{\rm out}/\varepsilon_{\rm mem})\}]+F_0L\varsigma\eta\times[(S_3/S_2)(\varepsilon_{\rm out}/\varepsilon_{\rm mem}-1)-1], \tag{14d}$$

with

$$S_3 = Q(\varsigma_1)/\varsigma_1 - Q(\varsigma_o)/\varsigma_o, \quad \varsigma_1 \cong \varsigma_o[1 - tb/\{a(a+b)\}]. \tag{14e}$$

In the above, $\varsigma = \varsigma_1$ represents the surface of the inner membrane, while the constant "*A*" is as

$$A = \frac{F_0 L[S_2(\varepsilon_{\text{in}} - \varepsilon_{\text{mem}}) + S_4(\varepsilon_{\text{out}} - \varepsilon_{\text{mem}}) - \varepsilon_{\text{in}} S_3(\varepsilon_{\text{out}}/\varepsilon_{\text{mem}} - 1)]}{S_2(\varepsilon_{\text{in}} - \varepsilon_{\text{mem}})Q(\varsigma_o)/\varsigma_o + (\varepsilon_{\text{in}} S_3 - \varepsilon_{\text{mem}} S_4)\{Q(\varsigma_o)/\varsigma_o - (\varepsilon_{\text{out}}/\varepsilon_{\text{mem}})dQ(\varsigma_o)/d\varsigma\}}, \tag{14f}$$

where

$$S_4 = dQ(\varsigma_1)/d\varsigma - Q(\varsigma_o)/\varsigma_o. \tag{14g}$$

The electric field normal to the outer ellipsoidal surface is $F_\varsigma(\varsigma, \eta)$, while $F_\eta(\varsigma, \eta)$ is orthogonal to F_ς and lies in planes containing the *z* axis. Expressions for these fields from Eqs. (13) are

$$F_\varsigma(\varsigma_o, \eta) = [(\varsigma_0^2 - 1)/(\varsigma_o^2 - \eta^2)]^{0.5}\{F_0 \eta - (A/L) \times [(Q(\varsigma_o) + \varsigma_o dQ(\varsigma_o)/d\varsigma)]\}, \tag{15a}$$

$$F_\eta(\varsigma_o, \eta) = [(1 - \eta^2)/(\varsigma_0^2 - \eta^2)]^{0.5}[F_0 \varsigma_o - AQ(\varsigma_o)/L]. \tag{15b}$$

For a spherical geometry, $a \to b$, and so $L \to 0$, $\varsigma_o \to \infty$ yielding $F_\varsigma = F_0 \cos(\phi)$, and $F_\eta = -F_0 \sin(\phi)$.

III. RESULTS AND DISCUSSION

Numerical calculations based on the equations of the previous section were performed to determined the effect of external electric fields on cellular shape changes. A list of parameters used in the computations are given in Table I. For accuracy the full stress theory [i.e., Eqs. (2) and (3)] was used without neglecting the bending forces and moments. A fourth-order Runge-Kutta method was used to numerically solve the resulting coupled differential equations. For self consistency, the electric fields at the surface for each geometrical shape had to be computed. This, in theory, can be accomplished by applying boundary conditions [Eq. (9)], and solving for all the Legendre-polynomial coefficients. However, such a procedure presents two practical difficulties. First, for successful numerical solution, a finite set of difference equations is needed. This implies having to invoke additional (perhaps arbitrary) conditions on the infinite Legendre series for closure. Second, evaluation of the normal derivatives [as in Eqs. 9(c)–(9d), for example] and radius of curvature [e.g., r_1 in Eqs. (2) and (3)] is "noisy" and leads to inaccuracies in numerical implementations. In order to circumvent the above difficulties, a slightly different approach was used here for the self-consistent analysis. A coupled iterative procedure was followed. First, Eqs. (2) and (3) were solved for the applied electric-field value (i.e., without self-consistent polarization corrections) to yield the deformed cell shape. Next, this shape was parametrized into an "ellipsoidal" form by a curve-fitting procedure that yielded the best-fit values of the semimajor and semiminor axes, *a* and *b*, respectively. The equations for the electric-field distribution for the ellipsoidal geometry [as given in Eqs. (14) and (15)], were then applied. This updated electric-field distribution was used once again to yield a more realistic shape based on Eqs. (2) and (3), and the process iterated until convergence. Obviously, since the deformed cell shape can, in principle, deviate appreciable from an ellipsoidal geometry at high electric fields (*E*) or large membrane thickness (*t*) values, the simulations were carried out for relatively small *E* and *t* magnitudes.

TABLE I. Parameters used for the simulations.

Parameter	Source	Value
k_{r1} ($F\ m^{-1}$)	Ref. [18]	$80 \times 8.85 \times 10^{-12}$
k_{r2} ($F\ m^{-1}$)	Ref. [18]	$2 \times 8.85 \times 10^{-12}$
a (m)	Ref. [15]	1×10^{-6}
t (m)	Ref. [15]	$(3-5) \times 10^{-9}$
K (J)	Ref. [54]	5×10^{-20}

Results for an initial spherical cell of thickness 2 nm having a 1 μm radius (typical of *E. coli* cells, for example) in response to various electric-field values are given in Fig. 3. Field magnitudes ranging from 0–70 kV/cm were used. The Poisson's ratio ν was taken to be 0.2. The steady-state deformed cell shapes for positive *z* and *y* variables in the $x = 0$ plane, are shown in Fig. 3. Due to the inherent symmetry of the problem, only the first quadrant is specified for simplicity. The shape changes from a perfect circle for $E = 0$ V/cm, to ellipsoidal with increasing eccentricity at higher fields. The corresponding forces per length $N_\phi(\phi)$ and $N_\theta(\phi)$ are shown in Fig. 4 for fields of 20, 50, and 70

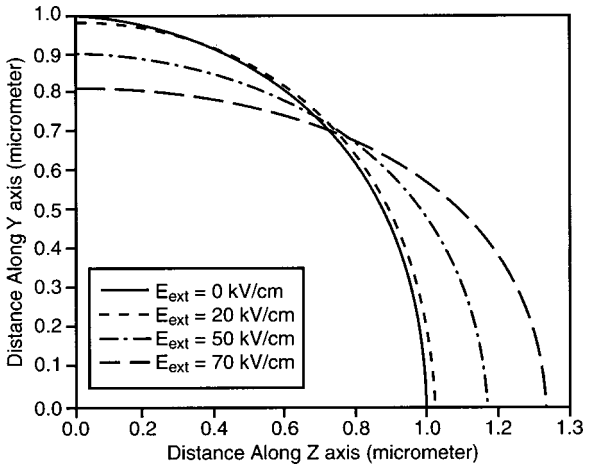

FIG. 3. Calculated equilibrium cell shapes along the *y-z* plane in response to applied electric fields of 0, 20, 50, and 70 kV/cm. Polarization effects were ignored.

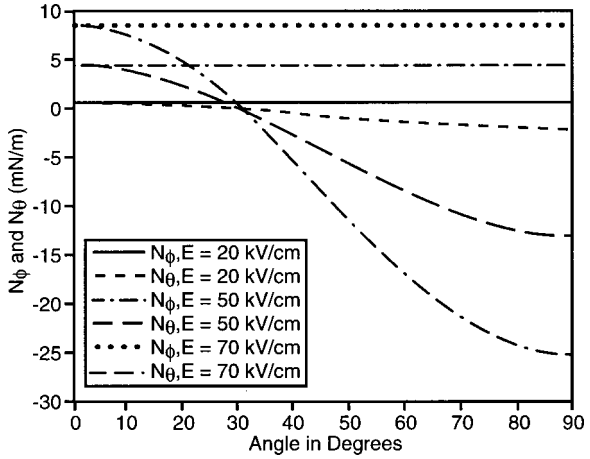

FIG. 4. Corresponding forces per length $N_\phi(\phi)$ and $N_\theta(\phi)$ for applied fields of 0, 20, 50, and 70 kV/cm.

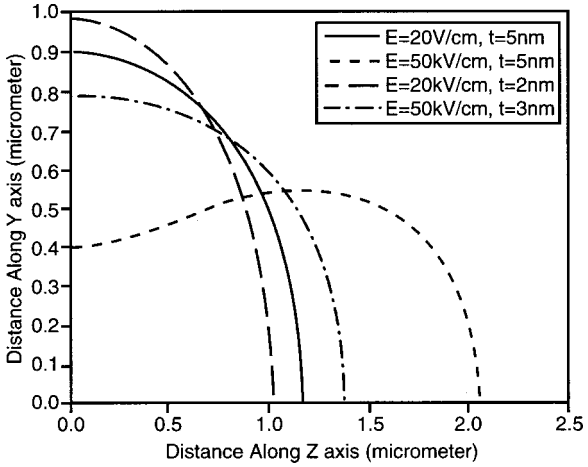

FIG. 5. Deformed cell shape results for various membrane thicknesses and applied fields of 20 kV/cm and 50 kV/cm.

kV/cm. The magnitudes range from 0 to about 25 mN/m. The values of N_ϕ are positive, independent of the angle, and increase with field. This implies that N_ϕ produces a constant tension across the membrane. Plots of $N_\theta(\phi)$ show positive magnitudes for angles below 30°, and become progressively negative reaching a maximum along the equatorial plane. The signs are simply the result of the chosen ϕ direction as depicted in Fig. 1. At low angles (i.e., close to the semimajor axis), positive $N_\theta(\phi)$ denotes a state of tension with component roughly transverse to the z axis. The negative values near $\phi \sim 90°$, for example, signifies a transverse (i.e., x-z plane) compression in response to the tension in the y-z plane. As reported in the literature [47], the typical tension for membrane rupture is in the range 1–10 mN/m. Our results are thus in very good agreement, and show that for applied electric fields of 50 kV/cm and higher, one can expect membrane rupture simply based on electromechanical considerations. The exact value will obviously depend on the rigidity parameter K and the Poisson's ratio ν, but the magnitudes as predicted by this simply analysis should roughly remain valid.

The deformed cell shape strongly depends on the cell characteristics. Changes in the rigidity parameter or the membrane thickness alter the force distributions, and hence, affect the overall shape. Calculated results of the deformed geometry for a 1μm radius starting from an unstressed spherical cell are given in Fig. 5. The membrane thickness ranged from 2–5 nm and various electric fields were used. The curves of Fig. 5 show very clearly that besides applied electric fields, the deformation is controlled by the membrane thickness, and increases with "t." As the thickness changes from 2 to 5 nm, the geometry is modified from spherical to ellipsoidal and then begins to assume a "peanut" shape (or discocyte transformation [38]). Based on the trend evident in Fig. 5, one could qualitatively predict an eventual shift towards a "dumbbell" geometry at higher fields, or thicker membranes, or under conditions of a smaller rigidity parameter, or with a larger Poisson's ratio. Such calculations for strongly deformed shapes, however, have not been shown here since the perturbative theory used in this analysis could be called into question for large deformations. In any case, it becomes evident that deviations from a simple geometry are indeed possible, and that the ellipsoidal form often used in previous work may not be the most accurate representation. It may also be mentioned that in actual practice, a slight change in the membrane thickness is likely during cellular deformation process. For example, a net expansion of the surface area would give rise to a marginal decrease in the membrane thickness "t." Based on the results of Fig. 5, such a "second-order" effect on "t" would work to slightly diminish the overall deformation.

Deviations in the electric-field distribution due to the presence of the dielectric media, are discussed next. The field profile for the components E_y and E_z are shown in Fig. 6 for a 1 μm radius spherical cell subjected to an external 20 kV/cm field was used, with relative permittivities of 81 and 2, respectively, for the membrane and surrounding media. Due to induced charges on the dielectric spherical membrane, the electric-field lines E_z deviate from their parallel orientation and tend to cluster at the cell. Consequently, the

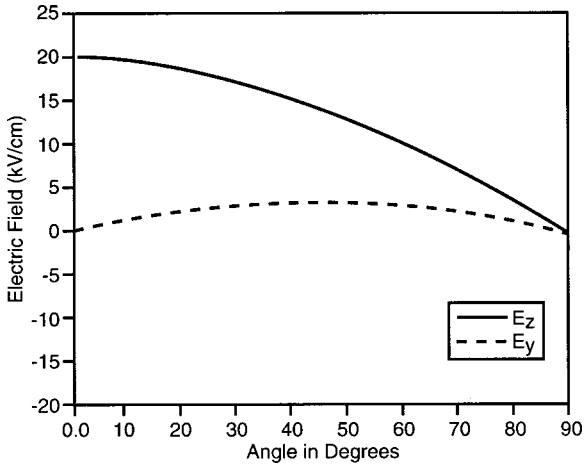

FIG. 6. Electric-field profiles just outside a 1 μm radius spherical cell in response to an external 20 kV/cm field. The relative permittivities for the membrane and surrounding media were set at 81 and 2, respectively.

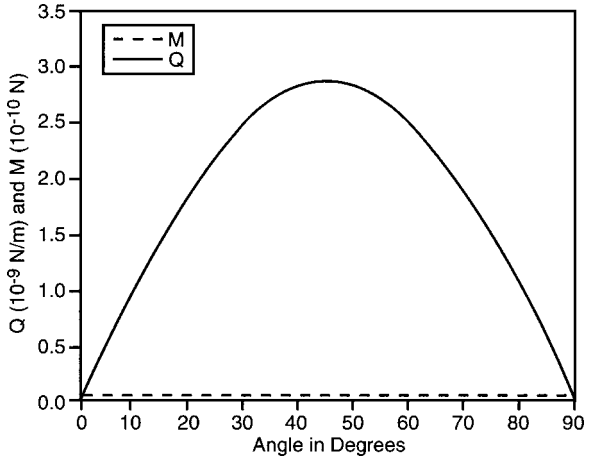

FIG. 7. The bending moment $M_\phi(\phi)$ and associated transverse force $Q_\phi(\phi)$ for applied field of 20 kV/cm for an initial 5 nm spheroid.

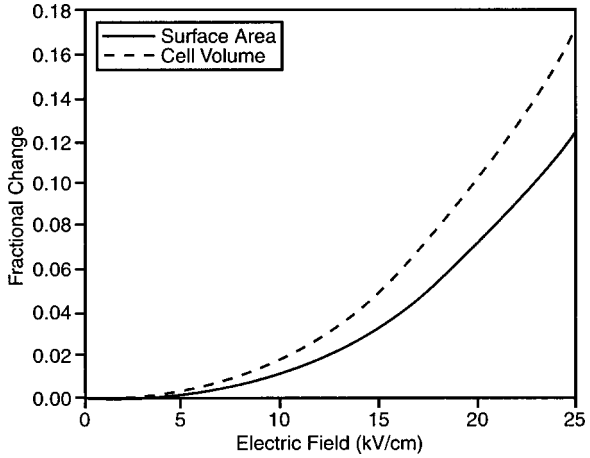

FIG. 8. Calculated variations in the cellular surface area and volume with applied electric field for an initial 1 μm cell radius and 5 nm membrane thickness.

radial field increases with the largest change from the 20 kV/cm value at the pole which corresponds to $\phi=0$. As expected, the radial component falls to zero at the equatorial plane which corresponds to $\phi=90°$. Due to the field distortion, the resultant field is no longer solely along the z direction, but instead has a small E_y component (largest at $\phi=45°$) and a deviation about the 20 kV/cm level in E_z. More significantly, the transverse component with polarization is smaller (i.e., less negative) which will lead to a decrease in the equatorial ''flattening.''

Finally, self-consistent numerical simulations were carried out to evaluate the field-dependent changes in the cell volume and surface area. The rationale for this calculation was the following: From an experimental standpoint, observations of absorbance dichroism and changes in optical scattering can be made, and these effects are associated with variability in cell surface area. It is, therefore possible to quantitatively observe and monitor areal changes and gauge the dependence on applied electric field through optical measurements. Analysis of such field-dependent variations is thus a meaningful first step towards comparisons with experiments, and for data interpretation.

Figure 7 shows the bending moment $M_\phi(\phi)$ and associated transverse force $Q_\phi(\phi)$ for an applied field of 20 kV/cm for an initial 5 nm sphere. As seen from the curve, the magnitude of $M_\phi(\phi)$ is negligibly small and has a nearly constant value of about 3×10^{-12} Newtons. The curve for $M_\theta(\phi)$ was nearly identical to that of $M_\phi(\phi)$, and so has not been shown separately in the figure. This $M_\theta(\phi)\sim M_\phi(\phi)$ condition obtained here is in keeping with a previous result reported by Pamplona and Calladine [48]. The angular dependence of $Q_\phi(\phi)$ from Fig. 7 is seen to be symmetric about $\phi=45°$, and also has a relatively small value. Thus, compared to both $N_\phi(\phi)$ and $N_\theta(\phi)$, the variables $Q_\phi(\phi)$, $M_\theta(\phi)$, and $M_\phi(\phi)$ can all be neglected as has been done in the past. Finally, Fig. 8 shows the fractional change in the cellular surface area and volume as a function of the applied electric field. Two points are evident from the results. First, both curves exhibit a rough quadratic behavior. This is in keeping with some recent optical scattering experimental data [28]. The exact magnitudes, however, are subject to the inaccuracies and uncertainty of the material parameters such as the rigidity K and Poisson's ratio ν. Hence, the data of Fig. 8 does not lend itself to a direct comparison with experimental data. However, the general electric-field-dependent trend predicted here has been shown to be accurate. A second point about Fig. 8 is that the change in cell volume is larger than the corresponding areal variation. This is to be expected as the volume scales more rapidly than the surface area, at least for the simple ellipsoidal shapes. At higher electric fields beyond the 25 kV/cm value shown in Fig. 8, it is conceivable that the areal variations become larger as the cell changes from an ellipsoidal to a ''peanut-discocyte geometry'' as shown in Fig. 5 for the 50 kV/cm field.

IV. SUMMARY AND CONCLUSIONS

A self-consistent model analysis of cellular deformation and shape change in response to an applied quasistatic electric field has been carried out. Such calculations would have direct applications to cellular electroporation, and provide an important step in the self-consistent evaluation of the electric field at the cell membrane. Accuracy in the electric-field values is important, since the field magnitude and distribution controls the pore formation rate, the evolution of the pore distribution function in ''r space'' as governed by the Smoluchowski equation, and ionic flow. As the fields are distorted by the polarizability of the biological medium and influenced by factors such as cellular size and geometric shape, an electromechanical analysis becomes necessary. Besides, experimental verification of such changes in cell shape could be probed through methods such as time domain dielectric spectroscopy [49] or microwave energy-loss measurements. These techniques accurately sample dynamic properties such as the dielectric permittivity, conductance, and capacitance of cells in suspension. The parameters are all governed by the cell geometry and shape. For example, on the basis of the Maxwell-Garnet theory [50,51], the collective dielectric be-

havior has been shown to depend on cell geometry [52], and could be extracted as a fitting parameter.

In this paper, the issue of calculating cell deformations self-consistently due to the electromechanical forces was presented. Instead of an energy-based virtual work formalism, a first-principles approach based on thin-shell theory was used. The difficulty with the virtual work method is that it does not lend itself to nonequilibrium analyses, or the inclusion of dissipative forces. An approach based on force and moment calculations has the advantage that it can potentially be extended to include dynamical analysis and temporal response. In this formulation, both the shear and bending moduli were carefully included, and the Love-Kirchhoff hypothesis used. Unlike most previous reports, assumptions such as constant surface area or cell volume have not been used. The present calculations demonstrated the following features: (i) At low values of the applied electric fields (as was commonly the case in the past), the deformed cells can roughly be approximated by an ellipsoidal shape. (ii) However, for much larger field magnitudes, as have recently been used [12–15], the deformations would be fairly significant and the cell geometry would no longer be described accurately by ellipsoidal shapes. For example, at fields on the order of 50 kV/cm, a ''peanut-shaped'' geometry was shown to result. The possibility of such discocytes had been predicted by Deuling and Helfrich [38]. (iii) The results here also demonstrated that the final shape depends on the membrane thickness. In general, it was argued that with decreasing thickness, deviations from the unstressed shape would be less severe. This has direct implications for cells, tissues, and lipid bilayers in which significant molecular reorientation and restructuring can occur upon the application of an electric field. (iv) Values of the surface forces obtained in the present calculations were in remarkably good agreement with the 1–10 mN/m range for membrane rupture that has been reported in the literature [47]. This lends validity and credence to the present paper. (v) It was also shown that, at least for the smaller electric fields, both the cellular surface area and volume would change roughly in a quadratic manner with electric field. (vi) Finally, it was shown that the bending moments are generally quite small and can be neglected for a simpler analysis.

The present paper lends itself to time-dependent analysis upon the inclusion of appropriate acceleration terms (linear and angular) in the force and moment balance equations. Thus, for example, situations such as cellular reorientation parallel to an applied field could be analyzed. This technique would also be applied to cells that had a nonspherical shape under unperturbed conditions (e.g., blood cells). Also, changes in the osmotic pressure could be included by incorporating a dynamical aspect to the p_r, p_ϕ, and p_θ variables. Obviously, for high-frequency temporal variations or ac excitations, the inclusion of Maxwell equations and Maxwell-Wagner polarization [53] would be needed. Such analyses will be presented elsewhere.

ACKNOWLEDGMENTS

The authors would like to thank S. Beebe (EVMS), L. Douglas Frink (Sandia National Laboratory), and W. Krassowska (Duke University) for useful discussions. This work was sponsored in part by the Air Force Office of Scientific Research (No. F49620-01-1-0506).

[1] R. Stampfli, An. Acad. Bras. Cienc. **30**, 57 (1958).
[2] T. Y. Tsongi, Biophys. J. **60**, 297 (1991).
[3] J. C. Weaver and Yu. A. Chizmadzhev, Bioelectrochem. Bioenerg. **41**, 135 (1996).
[4] I. G. Abidor, V. B. Arakelyan, L. V. Chernomordik, Y. A. Chizmadzhev, V. F. Pastushenko, and M. R. Tarasevich, Bioelectrochem. Bioenerg. **6**, 37 (1979).
[5] G. A. Hoffmann, S. B. Dev, and G. S. Nanda, IEEE Trans. Biomed. Eng. **46**, 752 (1999).
[6] D. C. Chang, B. M. Chassy, J. A. Saunders, and A. E. Sowers, *Guide to Electroporation and Electrofusion* (Academic, New York, 1992).
[7] E. Neumann, E. Sowers, and C. A. Jordan, *Electroporation and Electrofusion in Cell Biology* (Plenum, New York, 1989).
[8] S. Orlowski and L. M. Mir, Biochim. Biophys. Acta **1154**, 51 (1993).
[9] J. C. Weaver, J. Cell Biochem. Suppl. **51**, 426 (1993).
[10] A. J. H. Sale and W. A. Hamilton, Biochim. Biophys. Acta **148**, 781 (1967).
[11] H. Huelsheger, J. Potel, and E. G. Niemann, Radiat. Environ. Biophys. **20**, 53 (1981).
[12] K. H. Schoenbach, R. W. Alden III, and T. J. Fox, in *Conference Record of the 22nd International Power Modulator Symposium, Boca Raton, FL, 1996* (IEEE, Piscataway, NJ, 1996), p. 75.
[13] K. H. Schoenbach, F. E. Peterkin, R. W. Alden, and S. J. Beebe, IEEE Trans. Plasma Sci. **25**, 284 (1997).
[14] A. Ghazala and K. H. Schoenbach, IEEE Trans. Plasma Sci. **28**, 115 (2000).
[15] R. P. Joshi and K. H. Schoenbach, Phys. Rev. E **62**, 1025 (2000); R. P. Joshi, Q. Hu, R. Aly, K. H. Schoenbach, and H. P. Hjalmarson, *ibid.* **64**, 011913 (2001).
[16] K. H. Schoenbach, R. P. Joshi, R. H. Stark, F. Dobbs, and S. J. Beebe, IEEE Trans. Dielectr. Electr. Insul. **7**, 637 (2000).
[17] V. F. Pastushenko, Yu A. Chhizmadzhev, and V. B. Arakelyan, Bioelectrochem. Bioenerg. **6**, 53 (1979).
[18] S. A. Freeman, M. A. Wang, and J. C. Weaver, Biophys. J. **67**, 42 (1994); T. Vaughan and J. C. Weaver, *Electricity and Magnetism in Biology and Medicine*, edited by A. Bersani (Kluwer Academic, New York, 1999), p. 433.
[19] For example, L. D. Landau, E. M. Lifshitz, and L. P. Pitaevskii, *Electrodynamics of Continuous Media*, 2nd ed. (Pergamon, Oxford, 1984), pp. 39–42.
[20] H. P. Schwan, *Biological Effects and Dosimetry of Non-Ionizing Radiation* (Plenum, New York, 1983), pp. 213–231.
[21] U. Zimmermann, Biochim. Biophys. Acta **694**, 227 (1982).
[22] J. W. Ashe, D. K. Bogen, and S. Takashima, Ferroelectrics **86**, 311 (1988).
[23] K. H. Parker and C. P. Winlove, Biophys. J. **77**, 3096 (1999).

[24] J. W. Dai and M. P. Sheetz, Methods Cell Biol. **55**, 157 (1999).
[25] M. Golzio, M. P. Mora, C. Raynaud, C. Delteil, J. Teissie, and M. P. Rols, Biophys. J. **74**, 3015 (1998).
[26] H. Hotani, J. Mol. Biol. **178**, 113 (1984); T. Sekimura and H. Hotani, Forma **4**, 27 (1989).
[27] A. W. Friend, E. Finch, and H. P. Schwan, Science **187**, 357 (1975).
[28] E. Neumann, S. Kakorin, and K. Toensing, Faraday Discuss. **111**, 111 (1998).
[29] E. A. Evans, Biophys. J. **13**, 941 (1973).
[30] E. A. Evans and R. Skalak, *Mechanics and Thermodynamics of Biomembranes* (CRC, Boca Raton, 1980).
[31] J. C. Hansen, R. Skalak, S. Chien, and A. Hoger, Biophys. J. **72**, 2369 (1997).
[32] S. K. Boey, D. H. Boal, and D. E. Discher, Biophys. J. **75**, 1573 (1998).
[33] R. E. Waugh, J. Song, S. Svetina, and B. Zeks, Biophys. J. **61**, 974 (1992).
[34] B. Bozic, S. Svetina, and B. Zeks, Phys. Rev. E **55**, 5834 (1997).
[35] A. Iglic, J. Biomech. **30**, 35 (1997).
[36] K. Zeeman, H. Engelhard, and E. Sackman, Eur. Biophys. J. **18**, 203 (1990).
[37] W. Helfrich, Z. Naturforsch. A **28**, 693 (1973).
[38] H. J. Deuling and W. Helfrich, J. Phys. (France) **37**, 1335 (1976).
[39] B. K. Pai and H. D. Weymann, J. Biomech. **13**, 105 (1980).
[40] M. Kummrow and W. Helfrich, Phys. Rev. A **44**, 8356 (1991).
[41] V. L. Kononenko and J. K. Shimkus, Bioelectrochem. Bioenerg. **52**, 187 (2000).
[42] W. Flugge, *Stresses in Shells*, 2nd ed. (Springer, Berlin, 1962).
[43] S. Timoshenko and S. Woinowsky-Krieger, *Theory of Plates and Shells*, 2nd ed. (McGraw-Hill, New York, 1959).
[44] C. R. Calladine, *Theory of Shell Structures* (Cambridge University, Cambridge, 1983).
[45] N. Eynard, F. Rodriguez, J. Trotard, and J. Teissie, Biophys. J. **75**, 2587 (1998).
[46] For example, J. Van Bladel, *Electromagnetic Fields* (McGraw-Hill, New York, 1964).
[47] H. Isambert, Phys. Rev. Lett. **80**, 3404 (1998).
[48] D. C. Pamplona and C. R. Calladine, J. Biomed. Eng. **115**, 149 (1993).
[49] I. Ermolina, Y. Polevaya, Y. Feldman, B. Z. Ginzburg, and M. Schlesinger, IEEE Trans. Dielectr. Electr. Insul. **8**, 253 (2001).
[50] J. C. M. Garnett, Philos. Trans. R. Soc. London, Ser. B **203**, 385 (1904).
[51] R. Ruppin, Opt. Commun. **183**, 273 (2000).
[52] O. Levy and D. Stroud, Phys. Rev. B **56**, 8035 (1997).
[53] For example, J. A. Stratton, *Electromagnetic Theory* (McGraw-Hill, New York, 1941).
[54] E. Evans and W. Rawicz, Phys. Rev. Lett. **64**, 2094 (1990).